Evaluating a Concentrating Solar Power Plant as an Extended-Duration Peaking Resource

Kenjiro Yagi[a], Ramteen Sioshansi[a,*], Paul Denholm[b]

[a] *Department of Integrated Systems Engineering, The Ohio State University, 1971 Neil Avenue, Columbus, OH 43210-1271, United States of America*

[b] *Strategic Energy Analysis Center, National Renewable Energy Laboratory, 15013 Denver West Parkway, Golden, CO 80401-3305, United States of America*

Abstract

We explore the ability of a concentrating solar power (CSP) plant with thermal energy storage (TES) to provide peaking capacity. We focus on future power systems, wherein net load patterns may be significantly different than they are today (*e.g.*, due to higher renewable-energy penetrations). We examine 28 locations in the southwestern United States over an 18-year period. The hourly operation of the CSP plants are simulated to determine their potential to provide energy during an eight-hour peak-load window for each day up to 365 days per year. Our result shows that for the large majority of locations and years, CSP plants with certain configurations (*i.e.*, in terms of solar field and TES sizes) can provide nearly 100% peak-load capacity. We examine also the amount of supplemental energy (*e.g.*, by using natural gas as a supplemental thermal-energy source) that would be required to ensure that a CSP plant could serve the eight highest-load hours of every day of the year. We find that in most cases, a CSP plant supplemented with natural gas would require less than 5% of the fuel that is used by a natural-gas fired power plant providing the same level of reliable capacity. A series of sensitivity analyses show that these results are robust to the number of peak-load hours and days that are considered and the configuration of the CSP plant.

Keywords: Concentrating solar power, thermal energy storage, peaking generation, capacity value

1. Introduction

Concentrating solar power (CSP) plants can incorporate high-efficiency thermal energy storage (TES). In doing so, a CSP plant with TES can become a partially dispatchable source of renewable energy. Previous works, including those of Madaeni et al. (2012b, 2013); Usaola (2013), demonstrate that a CSP plant with TES has the potential to have a high capacity value, meaning that it can contribute to the power system serving load reliably. Many of these works use a limited number of years of data and focus on the availability of CSP generation during historical peak-load periods, which occur on hot summer afternoons in the southwestern United States. However, shifting demand patterns and contributions from other variable generation resources, such as solar photovoltaics (PV), may require examination of the contribution of CSP during other periods of the year.

In this work, we analyze 18 years of data from the southwestern United States to explore the ability of CSP to provide peaking capacity during extended periods of time. We deviate from the standard definition of capacity value, which uses historical data typically, thus focusing on only a few hours of the year. Instead, we explore the ability of CSP to provide firm capacity for eight hours per day, up to 365 days of the year. We calculate also the solar deficit, which is the amount of thermal energy that would need to be derived

*Corresponding author

Email addresses: yagi.7@osu.edu (Kenjiro Yagi), sioshansi.1@osu.edu (Ramteen Sioshansi), paul.denholm@nrel.gov (Paul Denholm)

from other resources to provide firm capacity. This solar deficit could be met by supplementing solar energy with other fuels or stored grid energy (*e.g.*, using resistive or inductive heaters to store energy in the CSP plant's TES system).

The remainder of this paper is structured as follows. Section 2 describes CSP technology briefly, including key sizing parameters, such as solar multiple and TES capacity. Section 3 describes our methods, including the performance metrics that we use to assess the ability of CSP to provide peaking capacity and the formulation of the model that is used in our analysis. Sections 4 and 5 summarize our case study data and results, respectively. Section 6 concludes.

2. CSP Technology

We consider the performance of power tower-type CSP plants, the technical characteristics of which are detailed by Mehos et al. (2016). Such plants consist of an array of heliostats, which typically is referred to as a solar field. The heliostats reflect the direct normal (beam) component of solar irradiance towards a central receiver. The concentrated solar energy heats a working fluid, which is typically molten salt, high-temperature oil, or water, that is within the receiver. In the case of a molten-salt working fluid, the heated salt is stored in a high-temperature insulated tank, which forms the storage medium for the TES system. The molten salt in such systems can be directed subsequently towards a salt-to-water heat exchanger, which produces steam to drive a conventional turbine or powerblock when energy is being discharged from the TES system.

Typically, the size of the powerblock is expressed by its rated capacity. This rated capacity can be given either as the maximum thermal power that can supplied to the powerblock (measured in MW-t) or its maximum electric output (measured in MW-e). If the capacity is measured by electric output, normally this is given as gross output. This is because typically CSP plants have parastic loads (*e.g.*, the tracking systems on the heliostats and the pumps that circulate the working fluid) that reduce the electric output of the plant. The size of a solar field is expressed often in terms of its solar multiple (SM). A solar field with an SM of 1.0 is sized to produce enough energy to drive the turbine at its rated output under design conditions, which are an instantaneous direct normal irradiance (DNI) of 950 W/m^2, a 5 m/s wind speed, and an ambient temperature of 25 C. Because these design conditions occur rarely (*e.g.*, one of the locations that we model achieves or exceeds these design conditions only in 6% of the hours of the year), an SM greater than 1.0 is typical, even for CSP plants without TES. For instance, the Ivanpah Solar Electric Generating System, which uses a direct steam receiver with no TES, has an SM of 1.4.[1] This is analogous to the dc/ac (or inverter loading) ratio of PV systems. Denholm et al. (2017) note that often PV systems have modules with a greater rating than the inverter, with the same underlying rationale as oversizing the solar field of a CSP plant relative to its powerblock.

As the SM increases, the thermal energy that is output from the solar field exceeds the turbine rating with increasing frequency. For a CSP plant with TES, this excess energy can be stored and used later. Doing so acts to increase the capacity factor of the CSP plant, while also reducing the plant's levelized cost of energy. As discussed by Sioshansi and Denholm (2010), the reason for this latter effect is that TES is typically a relatively small portion of the overall cost of a CSP plant (*e.g.*, estimated to be about 10% of the total direct capital cost of a CSP plant with an SM of 2.4 and a TES system with 10 hours of charging capacity). With an increased SM and sufficient TES, a CSP plant can be operated in a manner to ensure that it can provide energy when needed from a system-reliability perspective. In doing so, a system operator may depend on a CSP plant with TES to provide a 'firm' source of energy.

The energy storage capacity of a TES system may be measured in MWh-t. However, it is common to measure its capacity by the number of consecutive hours that the plant can operate at full output using only energy from a fully charged TES system. For example, the Solana Generating Station, which is a CSP plant

[1] The National Renewable Energy Laboratory maintains a database of CSP projects, which is publicly available at https://solarpaces.nrel.gov/. Unless noted otherwise, the technical and cost characteristics of existing CSP plants that we report are taken from this database.

with a parabolic trough design, has an SM of 2.0 and a TES system with six hours of TES. This means that if its TES system is charged fully, the plant can operate at its nameplate capacity for six consecutive hours using stored energy only. Plants with higher SMs and greater amounts of TES are also in operation. Collado and Guallar (2013) offer the Crescent Dunes Solar Energy Project, which has an SM of 2.0 and 12 hours of TES, and the Gemasolar Thermosolar Plant, which has an SM of 2.4 and 15 hours of TES as two such examples.

3. Methods

3.1. Overview

Our overarching goal in this work is to explore the ability of a CSP plant with TES to provide reliably peaking capacity in future power systems that may be dominated by renewable energy resources. The ability of a resource to provide capacity reliably is measured often using a reliability-based capacity-value metric, such as its effective load carrying capability (ELCC). For instance, Madaeni et al. (2012a, 2013) use ELCC as a metric to estimate the capacity value of CSP plants without and with TES systems, respectively. Usaola (2013) use ELCC and equivalent conventional power plant. Calculating the ELCC or equivalent conventional power plant (or most other reliability-based measures of capacity value) of a new resource requires performing a statistical analysis of the availability of all resources. In doing so, one can estimate how the new resource changes the likelihood of a supply shortfall within the system (*i.e.*, the loss of load probability). Loss of load probabilities are calculated typically over an extended period of time (*e.g.*, a year or more at hourly or subhourly intervals is common). DeSieno and Stine (1965); Garver (1966); Billinton and Allan (1984); Kariuki and Allan (1996) provide some of the formative works that develop reliability-based approaches to modeling capacity value.

Reliability-based approaches are accepted widely as providing robust estimates of the contribution of a new resource, including a CSP plant, to power system reliability. There are limitations to their use, however. First, they rely on a well defined power system mix, with known capacities and outage (failure) probabilities for each resource. Second, they depend on understanding daily and seasonal load patterns. In practice, ELCC and related calculations depend on and are highly sensitive to the operating profile of the new resource during only a relatively few peak-load periods of the year. These are typically hot weekday afternoons for much of the United States. As an extreme example, Madaeni et al. (2012a) demonstrate that under historical conditions, the examination of the output of a CSP plant during only the 10 highest-load hours of the year can provide an accurate assessment of its capacity value. Overall, ELCC or related formal capacity-value calculations rely heavily on historic conditions that may not reflect a future power system.

Considering the evolution of a power system, it can be quite challenging to project the power system mix, future load patterns, and the impact of variable generation resources, such as wind and solar, therein. Unlike traditional generation resources, the autocorrelation of solar and wind availability results in declining marginal capacity value as the penetrations of these resources rise. This is in addition to dramatic changes to the 'net load' patterns that must be met with dispatchable resources, such as a CSP plant with TES. Awara et al. (2018) demonstrate the decline in the marginal capacity value of solar PV as a function of its penetration. Given these complications, for this analysis, we perform a more general examination of the availability of the solar resource, as utilized by a CSP plant with TES. While less formal than traditional reliability-based approaches, the analysis that we conduct can provide insights into the ability of a CSP plant to provide firm capacity that are not as dependent on a particular generation mix or load profile.

Our performance metric examines the ability of a CSP plant with TES to provide full capacity during the eight highest-load hours of each day, while varying the number of days that is evaluated. In doing so, our analysis of the ability of a CSP plant to provide firm capacity is more robust to future net-load patterns, which may change due to the generation mix or underlying load of a power system. For comparison, currently the California Public Utilities Commission requires a resource to be able to generate for four continuous hours to provide full capacity credit under its resource adequacy program.[2] We calculate the shortfall of

[2] http://www.cpuc.ca.gov/WorkArea/DownloadAsset.aspx?id=6442454920

solar energy, which we term the 'solar deficit.' The solar deficit measures how much additional thermal energy would be needed to meet this eight-hour-output requirement over multiple days (ranging between one and 365 days). This shortfall could be used to understand whether a CSP plant could use an alternative fuel source (*e.g.*, natural gas, biofuels, or power system electricity that is stored in the TES system using inductive or resistive heaters) to meet the solar deficit.

We simulate the hourly performance of a power tower CSP plant with direct TES. This means that the heat-transfer fluid that drives the powerblock and the storage medium are the same molten salt. The molten salt is kept in a high-temperature insulated tank when thermal energy is stored in the TES system. The salt is circulated to the heat exchanger when the powerblock is operated and producing electricity. Our analysis consists of a two-step simulation approach, which we detail in the remainder of this section. First, we employ a physical model of the solar field of a hypothetical CSP plant to determine how much thermal energy it captures in each hour of each year that we simulate. Second, we use a mixed-integer linear optimization model to determine how the CSP plant should be operated to minimize its solar deficit in meeting the capacity criterion that we outline above. Our optimization model assumes perfect foresight of weather and load patterns. Zhang et al. (2019) show that solar forecasts are improving, but imperfect. Forecast errors introduce some uncertainty in the dispatch of CSP plants. To be conservative, we impose in our analysis the production requirement during the eight highest-load hours of the target days, which is longer than typical peak-load periods. This requirement allows for some uncertainty in the dispatch of the CSP plant. We also conduct a sensitivity analysis on this parameter in Section 5.5.

3.2. Physical Solar Field Model

We simulate the operation of the solar field using version 2017.1.17.r1 of System Advisor Model (SAM). Blair et al. (2018) provide a general description of SAM, summarizing its capabilities and use. SAM takes as an input hourly weather data and determines the amount of thermal energy that is collected by the receiver in the simulated CSP plant's tower. Depending on physical constraints (*i.e.*, the powerblock's thermal-input capacity and hours of storage in the TES system), this thermal energy either can be fed immediately into the powerblock to produce electricity or can be stored in the TES system.

3.3. Optimization Model

The second step adapts the mixed-integer linear optimization model of Sioshansi and Denholm (2010, 2013) to determine the operation of the CSP plant. The optimization model determines whether thermal energy that is collected by the solar field in each hour should be used to produce electricity or stored in the TES system. It also determines whether thermal energy that is stored in the TES system should be discharged in each hour to increase electricity production. SAM has the ability to dispatch CSP, but we opt to develop and use a customized optimization model. This is to ensure that the CSP plant achieves the goal of maximizing its production during the targeted eight-hour windows of peak demand. The optimization model is formulated to minimize the solar deficit over the course of the simulated year. The model has constraints that enforce the physical limits of the CSP plant and its TES. The constraints also restrict the CSP plant to use only the thermal energy that is gathered by its solar field, which is determined by SAM, and what is available from the TES. Additional discussion of the use of SAM and other optimization approaches to simulate CSP performance is provided by Martinek et al. (2018).

3.3.1. Optimization Model Nomenclature

We begin by defining notation for the optimization model.

Sets, Parameters, and Functions

E_t^{SF}	thermal energy collected from the solar field in hour t [MWh-t]
E^{SU}	energy consumed to startup the powerblock [MWh-t]
$F_t(\cdot,\cdot)$	hour-t powerblock heat-rate function [MWh-e]
H	hours of storage in TES system
K_t^p	hour-t solar-deficit penalty [$/MWh-t]
$P_t^{\mathrm{PB}}(\cdot,\cdot)$	hour-t powerblock parasitic load function [MWh-e]

P_t^{SF}	hour-t solar field parasitic load [MWh-e]
T	set of hourly time periods in the optimization horizon
$\Theta^{\max}$	maximum input to the powerblock when it is online [MWh-t]
$\Theta^{\min}$	minimum input to the powerblock when it is online [MWh-t]
Υ	self-discharge rate of TES system [p.u.]

We model the operation of the CSP plant over a set, T, of hourly time periods. K_t^p is a penalty parameter on having a solar deficit in hour t. The plant's solar field captures E_t^{SF} MWh-t of thermal energy in hour t. Operating the solar field imposes a parasitic load of P_t^{SF} MWh-e in hour t. This parasitic load is met by the powerblock's electric energy output during hours that it is producing and is provided by the power system during other hours. The thermal energy that is captured by the solar field can be used to produce energy from the powerblock, stored in the TES system, or released to ambient (*i.e.*, the energy that is collected can be curtailed).

For the powerblock to produce energy, it must be online. E^{SU} MWh-t of thermal energy must be consumed from combined solar field and TES output to switch the powerblock on from an offline state (*i.e.*, this thermal energy is not expended to keep on a powerblock that is already online). Any hour in which the powerblock is online, it must operate at between $\Theta^{\min}$ MWh-t and $\Theta^{\max}$ MWh-t of input energy (from combined solar field and TES output). The gross hour-t electric output of the powerblock is given by the heat rate function, $F_t(\cdot,\cdot)$, which depends on the amount of thermal energy that is input to the powerblock and the powerblock's online/offline state in hour t. The powerblock also has parasitic loads. The hour-t powerblock parasitic load is given by the function, $P_t^{\mathrm{PB}}(\cdot,\cdot)$, which depends also on the hour-t input thermal energy and online/offline state of the powerblock.

Because the CSP plant has a direct TES system, there are no power-capacity constraints on the charging and discharging of TES. There is an energy-capacity constraint. H represents the energy capacity of the TES system in terms of the number of consecutive hours that a fully charged TES system can be discharged to operate the powerblock at its thermal-input capacity. The TES system also has a self-discharge rate, Υ, which represents thermal energy that is lost over time.

Variables

l_t	ending hour-t state of charge of TES [MWh-t]
r_t	binary variable that equals 1 if the powerblock is started up in hour t and equals 0 otherwise
u_t	binary variable that equals 1 if the powerblock is online in hour t and equals 0 otherwise
θ_t	hour-t thermal energy input to the powerblock [MWh-t]
ω_t	hour-t net electric output of CSP plant [MWh-e]

r_t and u_t are binary variables that represent the start up and online states, respectively, of the powerblock in hour t. $r_t = 1$ if the powerblock is started up from an offline state in hour t and equals zero otherwise. $u_t = 1$ if the powerblock is online in hour t and equals zero otherwise. θ_t represents the amount of thermal energy that is input to the powerblock in hour t and ω_t is its net hour-t electric output. l_t is the ending hour-t state of charge of the TES system. There are no power-capacity limits on charging and discharging the TES system. Thus, we do not need variables that represent explicitly the amount of energy that is charged and discharged.

3.3.2. Optimization Model Formulation

The CSP-plant optimization model is formulated as:

$$\min \sum_{t\in T} K_t^p \cdot (\Theta^{\max} - \theta_t) \tag{1}$$

$$\text{s.t. } \Theta^{\min} u_t \le \theta_t \le \Theta^{\max} u_t - E^{\mathrm{SU}} r_t; \qquad \forall t \in T; \tag{2}$$

$$\omega_t = F_t(\theta_t, u_t) - P_t^{\mathrm{PB}}(\theta_t, u_t) - P_t^{\mathrm{SF}}; \qquad \forall t \in T; \tag{3}$$

$$r_t \ge u_t - u_{t-1}; \qquad \forall t \in T; \tag{4}$$

$$r_t \le 1 - u_{t-1}; \qquad \forall t \in T; \tag{5}$$

$$r_t \le u_t; \qquad \forall t \in T; \tag{6}$$

$$l_t \leq \Upsilon l_{t-1} + E_t^{\mathrm{SF}} - E^{\mathrm{SU}} r_t - \theta_t; \qquad \forall t \in T; \tag{7}$$
$$0 \leq l_t \leq H\Theta^{\max}; \qquad \forall t \in T; \tag{8}$$
$$u_t, r_t \in \{0, 1\}; \qquad \forall t \in T. \tag{9}$$

Objective function (1) measures the total penalty that is applied for any solar deficits. The hour-t solar deficit is defined as the difference between the nameplate input capacity of the powerblock and the amount of thermal energy that actually is delivered to the powerblock in hour t. Constraints (2) impose lower and upper limits on the amount of thermal energy that can be delivered to the powerblock when it is online. The maximum amount of thermal energy that can be delivered is reduced during hours in which the powerblock is started up. Otherwise, if the powerblock is offline in hour t, meaning that $u_t = 0$, then Constraint (2) for hour t forces zero thermal energy to be delivered to the powerblock. Constraints (3) define the net electrical output of the CSP plant as the gross electrical output, which is given by the heat-rate function, less the powerblock- and solar-field-parasitic loads. Constraints (4) define the values of the startup binary variables in terms of intertemporal changes in the values of the online binary variables. Constraints (5) and (6) impose additional restrictions on the values of the startup binary variables in terms of the values of the online binary variables.

Constraints (7) impose hourly thermal-energy balance and define implicitly the ending hourly state of charge of the TES system. The left-hand side of the hour-t constraint gives the ending hour-t state of charge of TES. The right-hand side gives the total amount of thermal energy that is available to be stored at the end of hour t, which gives the implicit upper bound on l_t. This bound is defined as sum of the amount of energy that is carried over from hour $(t-1)$, which, when accounting for thermal energy losses, is Υl_{t-1}, and energy that is collected by the solar field. From this amount of thermal energy that is available, the total amount of energy that is used to start the powerblock up, which is given by $E^{\mathrm{SU}} r_t$, and fed to the powerblock, which is given by θ_t, are subtracted. Constraints (8) impose state-of-charge limits on the TES system. Finally, Constraints (9) impose integrality on the online and startup state variables.

Following the work of Martinek et al. (2018), ramp rate constraints are not included in the formulation. This is because CSP plants can ramp over their full range in less than one hour. Moreover, our model does not consider additional value or benefits provided by rapid ramping for provision of ancillary services.

4. Case-Study Data

Our simulations are performed at 28 locations in the southwestern United States, which are illustrated in Figure 1. Table 1 provides coordinates for each location, which are grouped by the balancing authority area where they are located, as well as its annual-average daily DNI. We study a range of locations where CSP plants could be deployed, including some sites where CSP plants are already deployed or in planning stages.

We model power tower CSP plants and use default characteristics that are given in SAM. The default plant has a powerblock with a rated gross output capacity of 222 MW-e, which corresponds to a rated input capacity of 538 MW-t. Based on recent CSP-deployment trends, our analysis focuses on two solar-field and TES configurations. The first is a plant with an SM of 2.0 and six hours of TES while the second has an SM of 3.0 and 12 hours of TES. Following the work of Wagner et al. (2017), the heat-rate function is approximated as:

$$F_t(\theta_t, u_t) = \frac{1}{0.412} \eta_t^{amb} \cdot (0.4335 \cdot \theta_t - 11.345 \cdot u_t),$$

where η_t^{amb} is an hourly factor that accounts for the effect of the ambient temperature on powerblock efficiency.

The hourly solar-field parasitic loads, P_t^{SF}, are obtained directly from the SAM simulation that is used to determine E_t^{SF}. This is because the solar-field parasitic loads depend solely on the amount of energy that is required to operate the motors on the heliostats and have no dependence on how the TES or powerblock are operated. This can be contrasted with the powerblock-parasitic load, which depends on the operation of the plant and is determined by the optimization model (as opposed to by SAM) in our second modeling

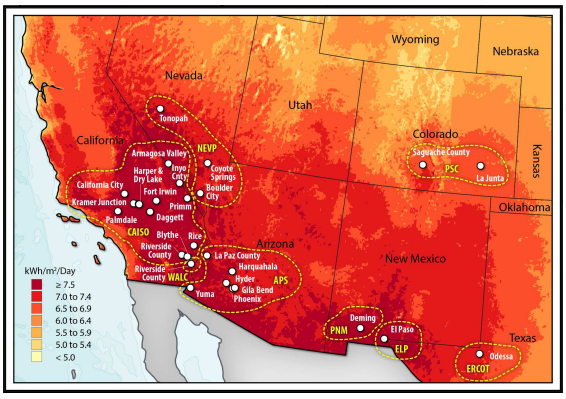

Figure 1: Map of 28 locations in the Southwestern United States that are studied and approximate boundaries of the balancing authority areas.

step. We estimate the powerblock-parasitic function by fitting a linear regression model to operating data that are obtained from SAM. A SAM simulation outputs the amount of thermal energy that is fed into the powerblock in each hour, which measures the extent to which the molten salt must be pumped in the plant and the condensers must operate, and the powerblock's hourly parasitic loads. The linear regression gives an estimate of $P_t^{\mathrm{PB}}(\theta_t, u_t)$, meaning that we can capture endogenously the effect of dispatch decisions on plant parasitics in the optimization.

We simulate plant operations over an 18-year period spanning 1998 through 2015. Weather data are obtained from version 2.0.1 of the National Solar Radiation Database (NSRDB). Sengupta et al. (2014a,b, 2018) describe the physical modeling that underlies production of the NSRDB while Wilcox (2012) provides a user manual for its use. We use historical load data, which are obtained from Federal Energy Regulatory Commission (FERC) Form 714 for each balancing authority area that is listed in Table 1, to determine the values of K_t^p in (1). K_t^p is set to \$1/MWh-t in the 16 lowest-load hours of each day and to \$1000/MWh-t in the remaining eight highest-load hours. This is to drive the plant to operate at its nameplate capacity during the eight highest-load hours of each day. There are seven balancing authority area/year combinations for which load data are not available from FERC. For these seven cases, we use load data from the nearest balancing authority area to set the values of K_t^p, taking into account any time-zone differences. Table 2 lists the seven cases in which load data are not available from FERC and the alternative balancing authority area that we use.

The optimization model that is detailed in Section 3.3 is formulated in `Python` 2.7 and solved using the version 7.5.1 of `Gurobi` on a system with an Intel Core i7-3630QM processor with four 3.40-GHz cores and 12 GB of memory. Default solver settings are used except for the optimality gap, which is set at 2% to reduce solution times. Each instance of the model, which is run over 13000 times to examine all location/year combinations and to conduct all of our sensitivity analyses, takes an average of between 12 s and 420 s of wall-clock time to run. The optimality-gap setting means that there may be feasible solutions that have smaller solar deficits. Thus, our results are up to 2% conservative in determining solar deficits.

5. Case-Study Results

5.1. Overview

Our primary performance metric is solar deficit, which is the shortfall in thermal energy that is needed to maintain nameplate output during the eight highest-load hours of the day. Section 5.2 demonstrates our approach by focusing on a single location. Section 5.3 broadens our results by summarizing all locations and years. Section 5.4 provides additional context for our results, by exploring how the solar deficit could be fulfilled using other energy sources. Finally, Section 5.5 examines the sensitivity of our results to the configuration of the CSP plant and the number of target hours during each day.

Table 1: Coordinates and annual-average DNI of 28 locations in the Southwestern United States that are studied, categorized by balancing authority areas.

Location Name	Coordinates	Annual-Average Daily DNI [kWh/m^2/day]
California Independent System Operator (CAISO)		
Fort Irwin, CA	35.26° N, 116.68° W	8.22
Kramer Junction, CA	35.01° N, 117.56° W	8.18
Rice, CA	34.07° N, 114.82° W	8.13
Harper Dry Lake, CA	35.03° N, 117.35° W	8.11
Armagosa Valley, NV	36.54° N, 116.52° W	8.00
Blythe, CA	33.67° N, 114.98° W	7.97
Harper Dry Lake, CA	35.02° N, 117.33° W	7.88
California City, CA	35.25° N, 118.01° W	7.86
Daggett, CA	34.86° N, 116.83° W	7.83
Primm, NV and CA	35.55° N, 115.46° W	7.81
Riverside County, CA	33.69° N, 115.22° W	7.79
Palmdale, CA	34.64° N, 118.11° W	7.61
Inyo County, CA	35.99° N, 115.90° W	7.60
Arizona Public Service Company (APS)		
Yuma, AZ	32.68° N, 114.62° W	7.97
La Paz County, AZ	33.83° N, 114.22° W	7.92
Hyder, AZ	33.06° N, 113.26° W	7.82
Harquahala, AZ	33.47° N, 113.11° W	7.82
Gila Bend, AZ	32.95° N, 112.89° W	7.67
Phoenix, AZ	32.92° N, 112.97° W	7.57
NV Energy (NEVP)		
Boulder City, NV	35.80° N, 114.98° W	7.60
Tonopah, NV	38.24° N, 117.36° W	7.52
Coyote Springs, NV	36.82° N, 114.93° W	7.52
Public Service Company of Colorado (PSC)		
La Junta, CO	37.98° N, 103.54° W	6.77
Saguache County, CO	37.84° N, 105.98° W	6.76
El Paso Electric Company (ELP)		
El Paso, TX	32.00° N, 106.77° W	8.12
PNM Resources (PNM)		
Deming, NM	32.26° N, 107.75° W	7.94
Western Area Lower Colorado (WALC)		
Riverside County, CA	33.46° N, 114.78° W	7.81
Electric Reliability Council of Texas (ERCOT)		
Odessa, TX	31.80° N, 103.00° W	7.32

5.2. Results for a Single Location

Figure 2 illustrates the general framework for analyzing our results. It shows the hourly operation of a CSP plant with an SM of 2.0 and six hours of TES that is located in Boulder City, NV on 1 July, 2014. It also shows the hourly loads for the corresponding balancing authority. The day that is shown has the highest load of the year. The two vertical bars in the figure indicate the eight-hour peak-load window on this day. The operation of the CSP plant is summarized by showing the amount of thermal energy that is collected by the solar field, the net electric output of the powerblock, and the state of charge of the TES in each hour. The day that is shown in Figure 2 has eight consecutive peak-load hours. However, our method does not impose the generation requirement during eight consecutive hours. Rather, it imposes the requirement

Table 2: Seven balancing authority area/year combinations for which load data are not available and alternative load data that are used.

Balancing Authority Area	Year	Alternate Balancing Authority Area
Arizona Public Service Company	2005	Western Area Lower Colorado
Electric Reliability Council of Texas	2001	El Paso Electric Company
Electric Reliability Council of Texas	2004	El Paso Electric Company
PNM Resources	2005	Western Area Lower Colorado
Public Service Company of Colorado	2005	Western Area Lower Colorado
Public Service Company of Colorado	2006	PNM Resources
California Independent System Operator	1998	Arizona Public Service Company

during the eight highest-load hours of the day. Thus, for example, if the load profile on a given day has two peaks (which often occurs during winter days, which have morning and evening peaks), the requirement is allocated across both periods.

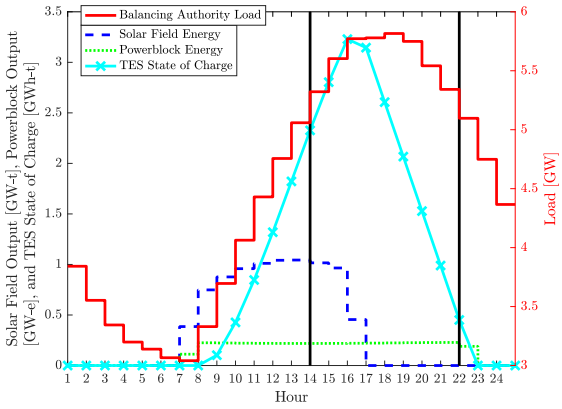

Figure 2: Thermal energy that is collected by the solar field, powerblock output, and state of charge of TES on 1 July, 2014 of a CSP plant in Boulder City, NV with an SM of 2.0 and six hours of TES and corresponding balancing-authority load. Solid vertical lines indicate the eight-hour peak-load window on this day.

On the day that is shown in Figure 2 the CSP plant operates at its nameplate capacity during the full eight-hour peak-load window. The operating patterns that are shown in the figure are typical for summer days with high demand. During mornings and early afternoons, thermal energy from the solar field exceeds the powerblock capacity. Thus, the plant both can generate at full output and store excess energy for later use. The figure shows the mismatch between solar field output, which peaks around hour 12, and demand, which peaks around hour 18. Energy from the solar field is available only for the first three to four hours of the peak-load window. Thus, the plant must draw on stored energy to generate at full capacity during the remaining hours of the peak-load window. This follows on previous results, which demonstrate that CSP plants can have very high capacity value as measured by their performance on peak-load days. The day that is shown in the figure likely has the highest probability of a generation shortfall (given that it has the highest demand of the year). Therefore, this is an extremely important day to analyze from the perspective of ensuring that the CSP plant can serve as a peaking resource. However, because our aim is to consider future power system scenarios, with varying contributions from different resources, we extend the analysis to all 365 days of the year.

Figure 3 shows results for 1 August, 2014, which is a day with lower demand but also lower solar availability. The two vertical bars in the figure indicate the eight-hour peak-load window on this day. Figure 3a shows that a CSP plant with an SM of 2.0 and six hours of TES cannot provide full output during our eight-hour peak-load window. It has a deficit of about 5.3% of the 4.3 GWh-t of thermal energy that

would be needed to meet our eight-hour peak-load window for the day, with the deficit occurring in hour 20. Interestingly, the CSP plant produces electricity in hours 9–12, which is before the peak-load window, because the six-hour TES system is saturated fully in hour 13. Thus, either the plant can curtail this excess thermal energy or produce outside of the peak-load window. For purposes of comparison, Figure 3b shows the operation of a CSP plant with an SM of 3.0 and 12 hours of TES. This plant can produce fully during the eight-hour peak-load window. Indeed, this plant is able to sustain some level of output in all of hours 1–20.

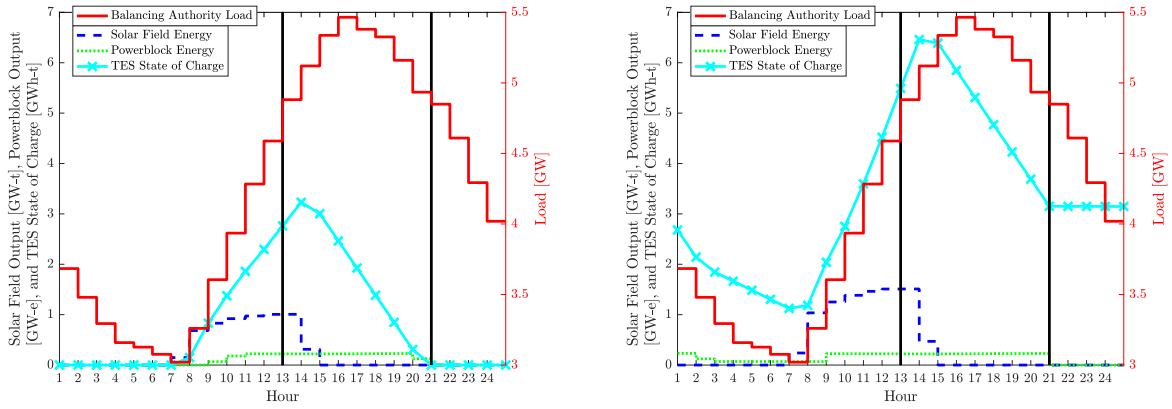

Figure 3: Thermal energy that is collected by the solar field, powerblock output, and state of charge of TES on 1 August, 2014 of a CSP plant in Boulder City, NV with (a) an SM of 2.0 and six hours of TES and (b) an SM of 3.0 and 12 hours of TES and corresponding balancing-authority load. Solid vertical lines indicate the eight-hour peak-load window on this day.

As we move from peak-load days, which are typically sunny in the southwestern United States, to lower-demand days, increasingly we experience cooler and potentially cloudy weather conditions. Figure 4 shows standard box plots of the annual solar deficit for a CSP plant in Boulder City, NV using all 18 years of case study data. The box plot is shown for different numbers of target days. For instance, 10 target days means that we seek to have the CSP plant operate at its nameplate capacity during the eight highest-load hours of the 10 days with the highest peak loads. The data in the figure are normalized as percentages of the total amount of thermal energy that is needed to meet the eight-hour peak-load window during the target days. This thermal energy requirement is about 4.3 GWh-t per day, which translates into a total of 1.57 TWh-t of thermal energy being needed to meet the eight-hour peak-load window if the requirement is imposed during all 365 days of the year (excluding energy that is required to startup the powerblock).

Figure 4b shows that a CSP plant with an SM of 3.0 and 12 hours of TES is able to meet effectively the eight-hour peak-load window during the 50 target days with the highest loads. Conversely, Figure 4a shows that a CSP plant with an SM of 2.0 and six hours of TES has a non-trivial solar deficit (of less than 5% of the total energy requirement) if considering the 50 target days with the highest loads. Thus, the capacity value of such a plant would likely be derated relative to its nameplate capacity. These findings follow previous analyses that demonstrate high capacity value for CSP plants with TES. As we consider lower-demand days, the CSP plant would need to draw energy from another source to supplement the thermal energy that is gathered by the solar field. In some extreme years, as much as 17% of the annual energy requirement would need to come from a supplemental source for a CSP plant with an SM of 2.0 and six hours of TES to meet the eight-hour peak-load window in all 365 days of the year. This requirement drops to about 6% for a CSP plant with an SM of 3.0 and 12 hours of TES.

5.3. Full Results

Figure 5 gives a broader feel for the results of our analysis by showing total annual solar deficits of CSP plants across the years and locations that are studied. The figure shows the solar deficits as percentages of the total amount of thermal energy that would be needed to meet the eight-hour peak-load window.

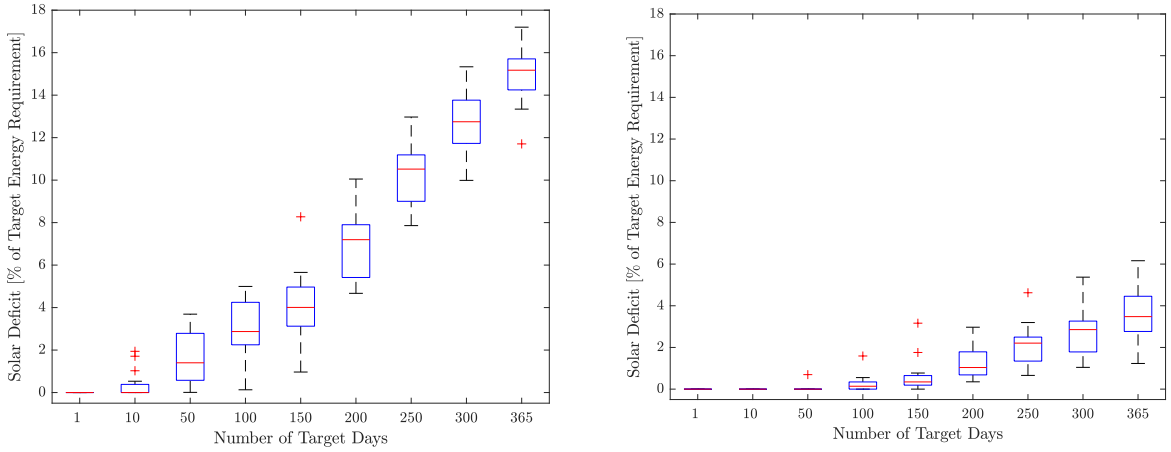

Figure 4: Standard box plots of total annual solar deficits as a percentage of target energy requirement across the years that are studied of a CSP plant in Boulder City, NV with (a) an SM of 2.0 and six hours of TES and (b) an SM of 3.0 and 12 hours of TES. Each box gives the 25th, 50th, and 75th percentiles, which we denote Q_{25}, Q_{50}, and Q_{75}, respectively. The whiskers represent the range of non-outlier observations, where outliers are defined as being less than $Q_{25} - 1.5(Q_{75} - Q_{25})$ or greater than $Q_{75} + 1.5(Q_{75} - Q_{25})$. Outliers are indicated with '+' signs.

Rather than plotting the solar deficits for all 28 locations, we show ranges for three clusters of locations that have different ranges of annual-average daily DNI. The figures demonstrate that for current power system conditions, wherein capacity value is dominated by the ability to generate on relatively few peak-load days of the year, CSP plants with at least six hours of TES can provide very high capacity value throughout the southwestern United States.

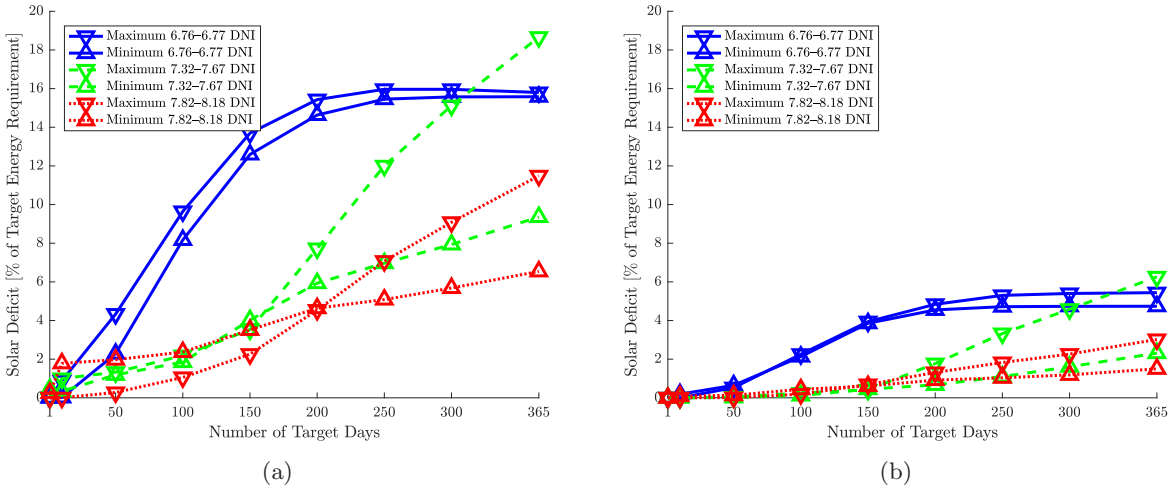

Figure 5: Ranges across the locations and years that are studied of total annual solar deficits as a percentage of target energy requirement of CSP plants with (a) an SM of 2.0 and six hours of TES and (b) an SM of 3.0 and 12 hours of TES, clustered by annual-average daily DNI of locations.

Most of the results in Figure 5 are clustered around a limited range, with a few clear exceptions. The solar deficit is monotonically increasing in the number of days analyzed for all locations, except for the two in Colorado (*i.e.*, the cluster with annual-average daily DNIs of 6.76 kWh/m^2/day–6.77 kWh/m^2/day). Colorado has somewhat different weather patterns, as well as lower DNI, compared to the other locations

that are analyzed. Colorado also has higher frequency of cold weather, with a number of high-demand days occurring in the winter. This produces the rapid rise in the solar deficit in Colorado compared to other regions (as seen in the figures for ranges of 50–200 days being analyzed).

The other location that has a relatively high solar deficit is Tonopah, NV. Tonopah, NV is the location with the highest solar deficit of the cluster with annual-average daily DNIs of 7.32 kWh/m^2/day–7.67 kWh/m^2/day. This location is the most northerly that we analyze and has many cloudy winter days. These characteristics of the location lead to lower CSP output during many lower-demand winter days, which gives rise to the higher solar deficit when evaluating a greater number of days.

Figure 5a shows also that DNI is not 'perfectly' correlated with solar deficit. The figure shows also that there are variations in correlation between annual DNI, seasonal DNI, and load patterns. For example, some locations with very good summer correlations (such as Harquahala, AZ, which is illustrated by the 'maximum' curve for the 7.82 kWh/m^2/day–8.18 kWh/m^2/day DNI range) have worse correlation in the winter, compared to the 'minimum' curve for the same DNI range (which corresponds to Rice, CA) which has somewhat better correlation in the winter and worse in the summer. We examine this in greater detail in Figures 6 and 7.

We would expect to observe a negative correlation between annual-average daily DNI and solar deficit. Figure 6 provides scatterplots showing the annual solar deficit versus the annual-average daily DNI, considering the 50 highest-load days of the year. The figures have two scatterplots each, with the circles representing each observation (*i.e.*, each location/year combination in our case study data) while the crosses represent the average (across the years that are studied) for each individual location. Figure 6a provides a scatterplot for a CSP plant with an SM of 2.0 and six hours of TES, while Figure 6b provides it for a plant with an SM of 3.0 and 12 hours of TES.

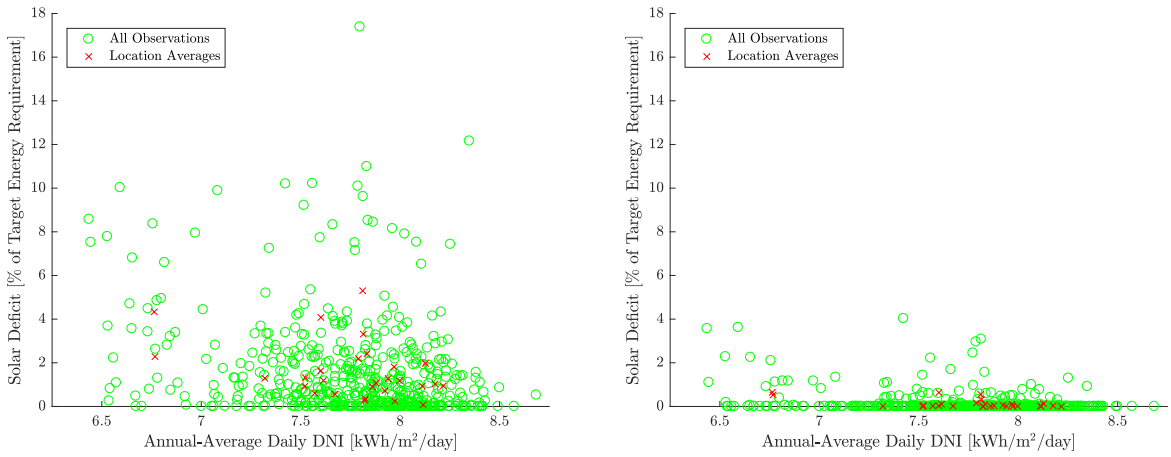

Figure 6: Scatterplot of total annual solar deficit across the 50 highest-load days of the year and annual-average daily DNI for CSP plants with (a) an SM of 2.0 and six hours of TES and (b) an SM of 3.0 and 12 hours of TES. The circles represent each observation while the crosses represent the average (across the years that are studied) for each location.

Surprisingly, Figure 6 does not show any clear relationship or pattern between the solar deficit and DNI. Figure 7 provides the same scatterplots that are in Figure 6. However, Figure 7 considers all days of each year. Interestingly, Figure 7 shows a more clear relationship between the solar deficit and DNI. These sets of scatterplots suggest that a CSP plant that is built at a lower-DNI location could essentially serve as a firm-capacity resource as effectively as a CSP plant that is at a higher-DNI location (within the range of DNIs that we analyze), if we restrict attention to a limited number of days (*e.g.*, 50 days in Figure 6). This is likely, at least in the immediate future. This result is because the TES provides flexibility in shifting solar energy from hours that are outside of the eight-hour peak-load window to the peak-load window. However, as more lower-load days, many of which tend to have lower DNI, are considered, the flexibility of the TES

system in shifting generation to meet the peak-load window is limited to a greater extent. This is because the solar field cannot collect sufficient energy to meet the peak-load window on such low-DNI days.

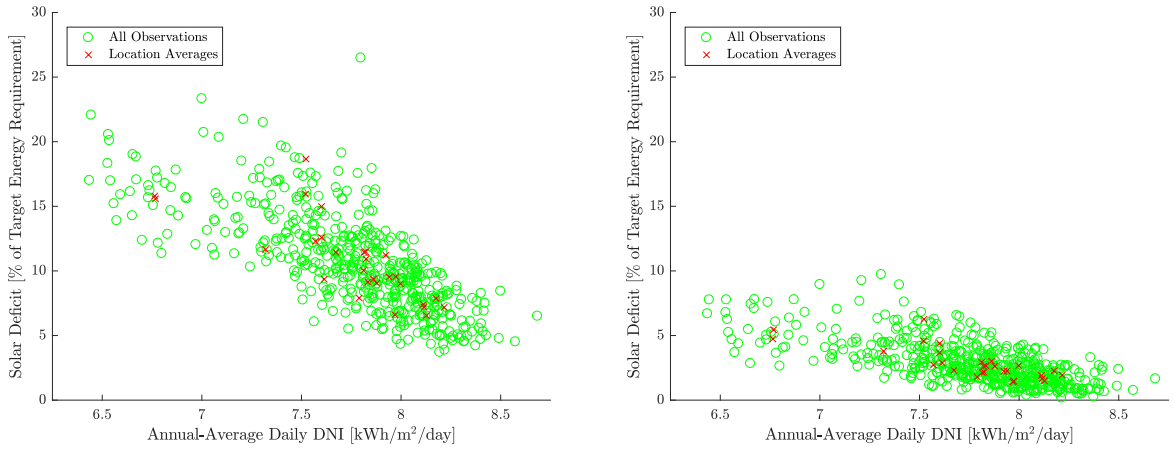

Figure 7: Scatterplot of total annual solar deficit across all days of the year and annual-average daily DNI for CSP plants with (a) an SM of 2.0 and six hours of TES and (b) an SM of 3.0 and 12 hours of TES. The circles represent each observation while the crosses represent the average (across the years that are studied) for each location.

There is considerable interannual variability in the results. However, much of this variability is due to weather variations during low-demand periods of time. Figure 8 shows ranges of the standard deviations (across the years that are studied) of the annual solar deficit for CSP plants with an SM of 3.0 and 12 hours of TES. The locations are clustered into the same groups that are used in Figure 5. Most locations have little interannual variation in the solar deficit if 100 or fewer highest-load days of the year are considered. However, the variation grows considerably as more days are considered. These results suggest also that if analyzing the peaking capability of CSP in today's power system, with requirements being determined by a small number of days, a single year's (or a limited number of years') data should provide relatively accurate results. As net load profiles change and other days become important to a larger extent, multiple years' data are needed to provide more robust estimates of peaking capability.

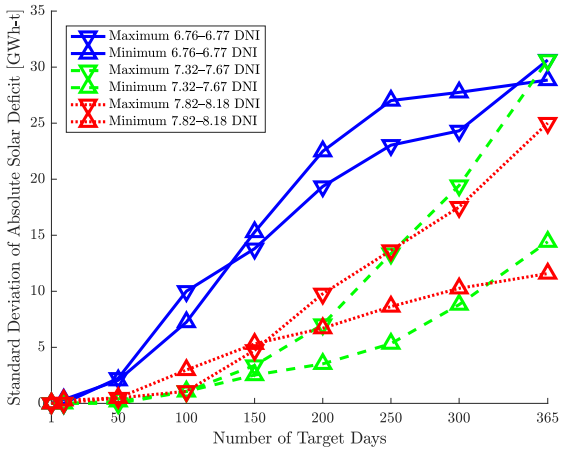

Figure 8: Ranges of standard deviation of total annual solar deficits of CSP plants with SM of 3.0 and 12 hours of TES, clustered by annual-average daily DNI of locations.

5.4. Supplementing Solar Energy for Improved Peaking Capability

The results in Sections 5.2 and 5.3 follow previous analyses, which show that CSP plants with TES can have relatively high capacity values under current power system conditions, wherein peaking capacity is needed mostly during a small number of peak-load periods. This is true of many parts of the southwestern United States, where some of the greatest challenges in serving load arise on hot sunny days with high air-conditioning loads. However, these results suggest also that significant shifts in net load patterns or other power system changes may require CSP plants to supplement solar thermal energy to ensure that they can provide peaking capacity. This is particularly true if CSP plants with a lower SM and fewer hours of TES are deployed.

There are two main pathways to supplement solar thermal energy in a CSP plant. One option is to store electric energy from the power system to mitigate any capacity shortfall. This can be done using resistive or inductive heaters to convert electricity into thermal energy that can be stored in the TES system. The thermal efficiencies of resistive or inductive heaters are near 100%. However, the overall round-trip efficiency of this approach is well under 50%. This is because the overall conversion efficiency is limited by the efficiency of the Rankine cycle, which is about 42% in our analysis.

If this approach is pursued, the energy that is stored could be derived from any conventional or renewable source that is integrated in the power system. If the overarching goal is to store primarily renewable energy, such as PV or wind, in the TES system, careful analysis is required to determine the availability of such resources. To illustrate this challenge, Figure 9 shows the daily solar deficit for Boulder City, NV in 2014 for the two CSP-plant configurations that we analyze. These deficits would require supplemental energy to maintain full CSP output during the eight-hour peak-load window of each day. Many of the deficit days occur during the winter, implying limited solar PV availability, at least in close proximity to the CSP plant. Alternatively, there may be significant wind availability, particularly in the spring. With sufficient transmission capacity, this may allow a CSP plant to act as an additional mechanism to store otherwise curtailed wind energy, albeit at a lower round-trip efficiency than other energy storage technologies.

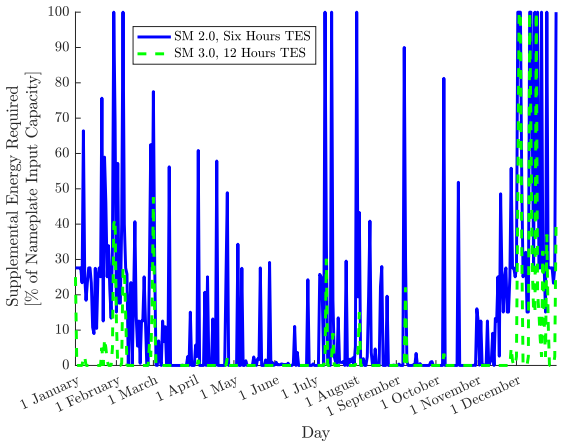

Figure 9: Daily supplemental thermal energy needed for a CSP plant in Boulder City, NV to meet the eight-hour peak-load window in 2014.

A second option is to add a supplemental combustible fuel source to the CSP plant. Conventional CSP plants use Rankine steam cycles. Thus, solar thermal energy can be augmented using duct burners, which heat the steam through the combustion of natural gas. This increases the peaking capability of a CSP plant to be equivalent to that of a natural gas-fired unit, insomuch as the ability of the CSP plant to produce during peak-load periods is limited only by natural gas availability and the forced outage rate of the plant. Disadvantages to this approach include an increase in plant cost as well as in fuel use and associated emissions.

We can use the solar deficit calculations that are summarized in Sections 5.2 and 5.3 to determine the impact of adding natural gas-combustion capabilities to the CSP plants that we analyze. Specifically,

we can estimate fuel use and emissions and compare them to the fuel use and emissions of a natural gas-fired generating unit. For example, assuming the 85% net thermal efficiency of natural gas combustion that Peterseim et al. (2016) employ in their work, each GWh-t of solar deficit requires about 4.2 TJ (4014 MMBTU) of natural gas, which would produce 213 tons of CO_2 emissions.

Figure 10 summarizes the impact of using supplemental natural gas to meet the eight-hour peak-load window with a CSP plant and contrasts it with the impact of using a natural gas-fired unit. Rather than showing results for all 28 locations, we show the locations with the most and least supplemental energy needs and the average of the 22 locations with annual-average daily DNIs of 7.5 kWh/m^2/day–8.0 kWh/m^2/day. The left-hand axis of the figure shows annual natural gas use as a function of the number of days on which the peak-load window is met. The right-hand axis shows the associated CO_2 emissions. The figure shows also the fuel use and emissions if the eight-hour peak-load window is met entirely from a natural gas-fired plant. We assume two efficiencies—35%, which corresponds to a simple-cycle unit, and 55%, which corresponds to a combined-cycle unit.

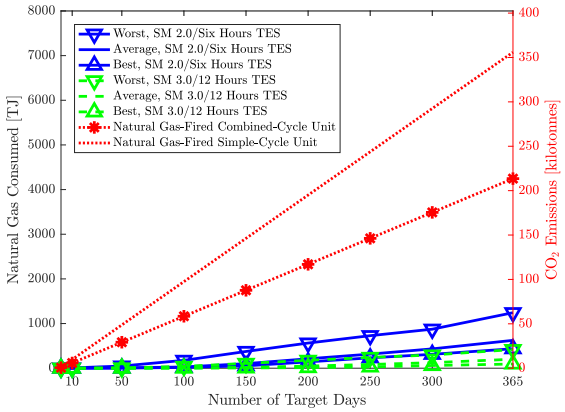

Figure 10: Supplemental natural gas requirement and resulting emissions to meet eight-hour peak-load window with a CSP plant and with combined- and simple-cycle natural gas-fired generating units.

The results in Figure 10 indicate that a CSP plant with an SM of 2.0 and six hours of TES that is located in a typical-resource location in the southwestern United States (*i.e.*, with an annual-average daily DNI of 7.5 kWh/m^2/day–8.0 kWh/m^2/day) can avoid both the construction of a natural gas-fired plant (due to its high capacity credit) and the majority of its fuel use and resulting emissions. For example, supplementing a CSP plant with an SM of 2.0 and six hours of TES with natural gas to ensure reliable peaking capability during the 100 highest-demand days would use no more than about 4% of the fuel that would be consumed by a natural gas-fired plant. A plant with an SM of 3.0 and 12 hours of TES would use no more than about 5% of the fuel that is consumed by a natural gas-fired unit even if the peak-load requirement is extended to all of the days of the year. These relatively modest fuel usages also increase opportunities to use renewably derived gas or liquid fuels for supplemental energy to produce an entirely renewable generation source.

5.5. Sensitivity Analyses

We summarize the results of three sensitivity analyses in this section. First, we examine the effect of varying the number of target hours during which the plant must be operating at its nameplate capacity in each day to be six and 10 hours. Figure 11 is a standard box plot showing the case of CSP plants with an SM of 3.0 and 12 hours of TES. In case of 50 target days (which is shown in the left-hand half of the figure), for the majority of location/year combinations, the solar deficit is near-zero regardless of the number of target hours. Moving to the most extreme case of imposing the requirement in all 365 days (which is shown in the right-hand side of the figure), the solar deficit increases typically by about one percentage point if imposing the requirement during the 10 highest-load hours of each day.

Second, we show the effect of having different amounts of TES capacity. Figure 12 provides box plots summarizing the energy deficits of CSP plants that have SMs of 3.0 and with different TES capacities.

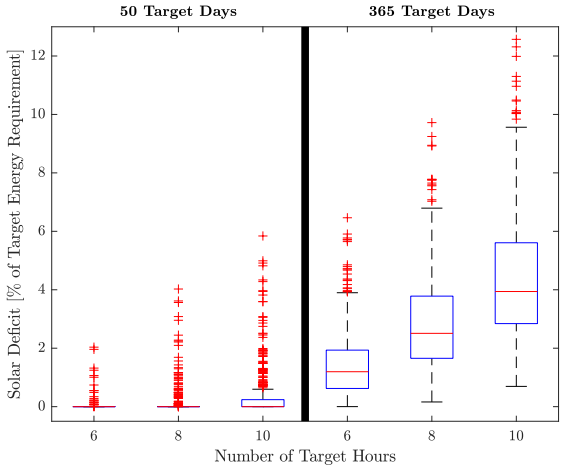

Figure 11: Standard box plots of total annual solar deficits as percentages of target energy requirement across the years and locations that are studied of a CSP plant with SM of 3.0 and 12 hours of TES and different numbers of target hours and days. Each box gives the 25th, 50th, and 75th percentiles, which we denote Q_{25}, Q_{50}, and Q_{75}, respectively. The whiskers represent the range of non-outlier observations, where outliers are defined as being less than $Q_{25} - 1.5(Q_{75} - Q_{25})$ or greater than $Q_{75} + 1.5(Q_{75} - Q_{25})$. Outliers are indicated with '+' signs.

As before, all 504 location/year combinations are summarized in the box plots and results are shown for imposing the peaking requirement during both the 50 and 365 highest-load days of the year (on the left- and right-hand sides, respectively, of the figure). The figure shows that for many cases, the solar deficit is near-zero regardless of TES size, but both numbers of target days show a substantial increase in solar deficit with reduced hours of TES in some cases.

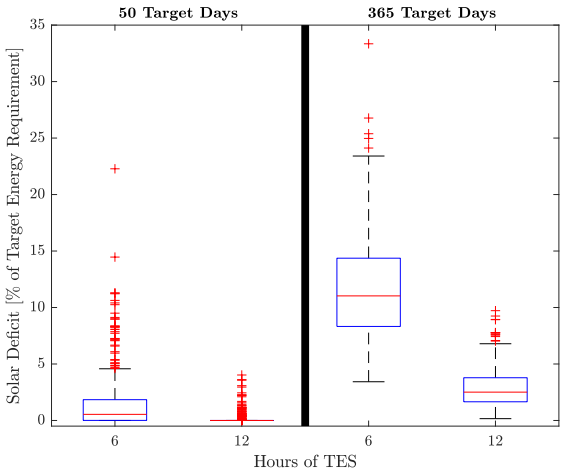

Figure 12: Standard box plots of total annual solar deficits as percentages of target energy requirement across the years and locations that are studied of a CSP plant with SM of 3.0 with eight target hours and different numbers of target days and hours of TES. Each box gives the 25th, 50th, and 75th percentiles, which we denote Q_{25}, Q_{50}, and Q_{75}, respectively. The whiskers represent the range of non-outlier observations, where outliers are defined as being less than $Q_{25} - 1.5(Q_{75} - Q_{25})$ or greater than $Q_{75} + 1.5(Q_{75} - Q_{25})$. Outliers are indicated with '+' signs.

Lastly, we examine the effect of a CSP plant's SM on its solar deficit. Figure 13 shows standard box plots for solar deficits for CSP plants with 12 hours of TES and with the original eight-hour requirement imposed during the 50 and 365 highest-load days of the year (in left- and right-hand sides, respectively, of the figure), while varying the SM. Overall, few of the cases show dramatic changes in the results.

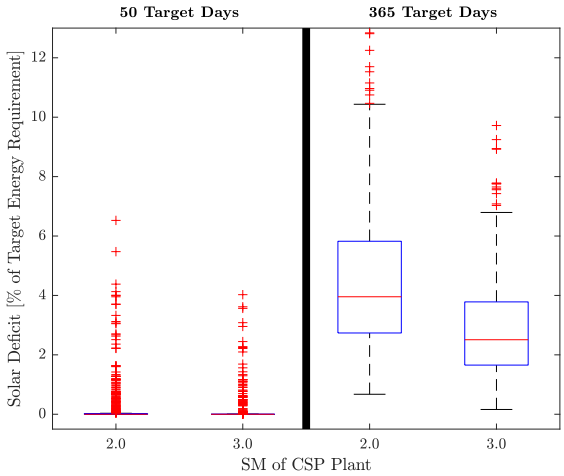

Figure 13: Standard box plots of total annual solar deficits as percentages of target energy requirement across the years and locations that are studied of a CSP plant with 12 hours of TES, eight target hours, and different numbers of target days and plant SMs. Each box gives the 25th, 50th, and 75th percentiles, which we denote Q_{25}, Q_{50}, and Q_{75}, respectively. The whiskers represent the range of non-outlier observations, where outliers are defined as being less than $Q_{25} - 1.5(Q_{75} - Q_{25})$ or greater than $Q_{75} + 1.5(Q_{75} - Q_{25})$. Outliers are indicated with '+' signs.

The results of these sensitivity analyses should be considered as part of overall plant-design considerations. Plant design should account for cost and benefits, which may include avoided system capacity and the need for 'makeup' energy to address solar deficits.

6. Discussion and Conclusions

Well established methods demonstrate that CSP plants with TES can provide capacity value that is similar to that of conventional plants. Our analysis uses multiple years of data at multiple sites to confirm the availability of significant solar energy during nearly every high-demand day. This solar availability, combined with at least six hours of TES, supports high capacity value for CSP plants throughout the southwestern United States.

An outstanding question is what happens if and when large amounts of PV or wind or other changes in demand alter the shape of demand patterns. Using multiple years' data demonstrates that there may be a shortfall in energy due to the need for peaking capacity during cloudy winter days. This energy could be derived from energy that is stored from the power system, or by supplementing solar thermal energy with natural gas firing. The amount of natural gas that would be consumed is less than 5% of that which is used by a natural gas-fired unit when considering the 100 highest-load days for a CSP plant with an SM of 2.0 and six hours of TES. A CSP plant with an SM of 3.0 and 12 hours of TES has the same 5% energy deficit to meet the peak-load window during every day of the year.

In the near term, peaking-capacity resources are not needed for anywhere close to all 365 days of the year. As discussed above, analyses of many resources (both renewable and conventional) find that only a relatively few days of the year drive reliability assessments. However, the use of a thermal generation cycle is a realistic and potentially cost-effective mechanism to ensure that a CSP plant can provide cromulent peaking capacity, while maintaining the majority of its fuel-reduction benefits.

Acknowledgments

This work was authored, in part, by the National Renewable Energy Laboratory, which is operated by Alliance for Sustainable Energy, LLC, for the United States Department of Energy (DOE) under contract number DE-AC36-08GO28308. Funding was provided by the DOE Office of Energy Efficiency and Renewable

Energy Solar Energy Technologies Office. The views expressed in the article do not necessarily represent the views of the DOE or the United States Government. The United States Government retains and the publisher, by accepting the article for publication, acknowledges that the United States Government retains a nonexclusive, paid-up, irrevocable, worldwide license to publish or reproduce the published form of this work, or allow others to do so, for government purposes.

The authors thank three anonymous reviewers, the editors, Mark Mehos, Craig Turchi, Jeffrey Logan, Aaron Bloom, and Armin Sorooshian for helpful discussions, comments, and suggestions. Billy Roberts provided invaluable assistance in developing Figure 1. The material in this paper is based upon work that was financially supported by the Alliance for Sustainable Energy, LLC through subcontract XEJ-7-70018-01. The first author thanks Tokushu Tokai Paper Co., Ltd. for its financial support for his Ph.D. studies at The Ohio State University. Any opinions and conclusions that are expressed in this paper are solely those of the authors. Devonie McCamey provided editorial assistance. Any remaining errors are entirely those of the authors.

References

Awara, S., Zareipour, H., Knight, A., 13-16 May 2018. Solar Power Capacity Value Evaluation—A Review. In: 2018 IEEE Canadian Conference on Electrical & Computer Engineering. Institute of Electrical and Electronics Engineers, Quebec City, Quebec, Canada.

Billinton, R., Allan, R. N., 1984. Reliability Evaluation of Power Systems. Pitman Advanced Publishing Program, Boston, Massachusetts.

Blair, N., DiOrio, N., Freeman, J., Gilman, P., Janzou, S., Neises, T., Wagner, M., May 2018. System Advisor Model (SAM) General Description (Version 2017.9.5). Tech. Rep. NREL/TP-6A20-70414, National Renewable Energy Laboratory, Golden, CO.

Collado, F. J., Guallar, J., April 2013. A review of optimized design layouts for solar power tower plants with *campo* code. Renewable and Sustainable Energy Reviews 20, 142–154.

Denholm, P., Eichman, J., Margolis, R., August 2017. Evaluating the Technical and Economic Performance of PV Plus Storage Power Plants. Tech. Rep. NREL/TP-6A20-68737, National Renewable Energy Laboratory, Golden, CO.

DeSieno, C. F., Stine, L. L., March 1965. A Probability Method for Determining the Reliability of Electric Power Systems. IEEE Transactions on Reliability R-14, 30–35.

Garver, L. L., August 1966. Effective Load Carrying Capability of Generating Units. IEEE Transactions on Power Apparatus and Systems PAS-85, 910–919.

Kariuki, K. K., Allan, R. N., March 1996. Evaluation of reliability worth and value of lost load. IEE Proceedings—Generation, Transmission, and Distribution 143, 171–180.

Madaeni, S. H., Sioshansi, R., Denholm, P., May 2012a. Estimating the Capacity Value of Concentrating Solar Power Plants: A Case Study of the Southwestern United States. IEEE Transactions on Power Systems 27, 1116–1124.

Madaeni, S. H., Sioshansi, R., Denholm, P., February 2012b. How Thermal Energy Storage Enhances the Economic Viability of Concentrating Solar Power. Proceedings of the IEEE 100, 335–347.

Madaeni, S. H., Sioshansi, R., Denholm, P., May 2013. Estimating the Capacity Value of Concentrating Solar Power Plants with Thermal Energy Storage: A Case Study of the Southwestern United States. IEEE Transactions on Power Systems 28, 1205–1215.

Martinek, J., Jorgenson, J., Mehos, M., Denholm, P., 1 December 2018. A comparison of price-taker and production cost models for determining system value, revenue, and scheduling of concentrating solar power plants. Applied Energy 231, 854–865.

Mehos, M., Turchi, C., Jorgenson, J., Denholm, P., Ho, C., Armijo, K., May 2016. Advancing Concentrating Solar Power Technology, Performance, and Dispatchability. Tech. Rep. NREL/TP-5500-65688, National Renewable Energy Laboratory, Golden, CO.

Peterseim, J. H., Viscuso, L., Hellwig, U., McIntyre, P., 1 May 2016. Large capacity, multi-fuel, and high temperature working fluid heaters to optimize CSP plant cost, complexity and annual generation. In: Rajpaul, V., Richter, C. (Eds.), AIP Conference Proceedings. Vol. 1734. American Institute of Physics, Cape Town, South Africa.

Sengupta, M., Habte, A., Gotseff, P., Weekley, A., Lopez, A., Anderberg, M., Molling, C., Heidinger, A., September 2014a. A Physics-Based GOES Product for Use in NREL's National Solar Radiation Database. Tech. Rep. NREL/CP-5D00-62776, National Renewable Energy Laboratory, Golden, CO.

Sengupta, M., Habte, A., Gotseff, P., Weekley, A., Lopez, A., Molling, C., Heidinger, A., July 2014b. A Physics-Based GOES Satellite Product for Use in NREL's National Solar Radiation Database. Tech. Rep. NREL/CP-5D00-62237, National Renewable Energy Laboratory, Golden, CO.

Sengupta, M., Xie, Y., Lopez, A., Habte, A., Maclaurin, G., Shelby, J., June 2018. The National Solar Radiation Data Base (NSRDB). Renewable and Sustainable Energy Reviews 89, 51–60.

Sioshansi, R., Denholm, P., October 2010. The Value of Concentrating Solar Power and Thermal Energy Storage. IEEE Transactions on Sustainable Energy 1, 173–183.

Sioshansi, R., Denholm, P., October 2013. Benefits of Colocating Concentrating Solar Power and Wind. IEEE Transactions on Sustainable Energy 4, 877–885.

Usaola, J., November 2013. Capacity credit of concentrating solar power. IET Renewable Power Generation 7, 680–688.
Wagner, M. J., Newman, A. M., Hamilton, W. T., Braun, R. J., 1 October 2017. Optimized dispatch in a first-principles concentrating solar power production model. Applied Energy 203, 959–971.
Wilcox, S. M., August 2012. National Solar Radiation Database 1991-2010 Update: User's Manual. Tech. Rep. NREL/TP-5500-54824, National Renewable Energy Laboratory, Golden, CO.
Zhang, X., Li, Y., Lu, S., Hamann, H. F., Hodge, B.-M., Lehman, B., January 2019. A Solar Time Based Analog Ensemble Method for Regional Solar Power Forecasting. IEEE Transactions on Sustainable Energy 10, 268–279.